Accelerating the photocatalytic water splitting in catalyst-dye complexes

Shao, Y.

CHAPTER 1

Introduction & Computational Tools

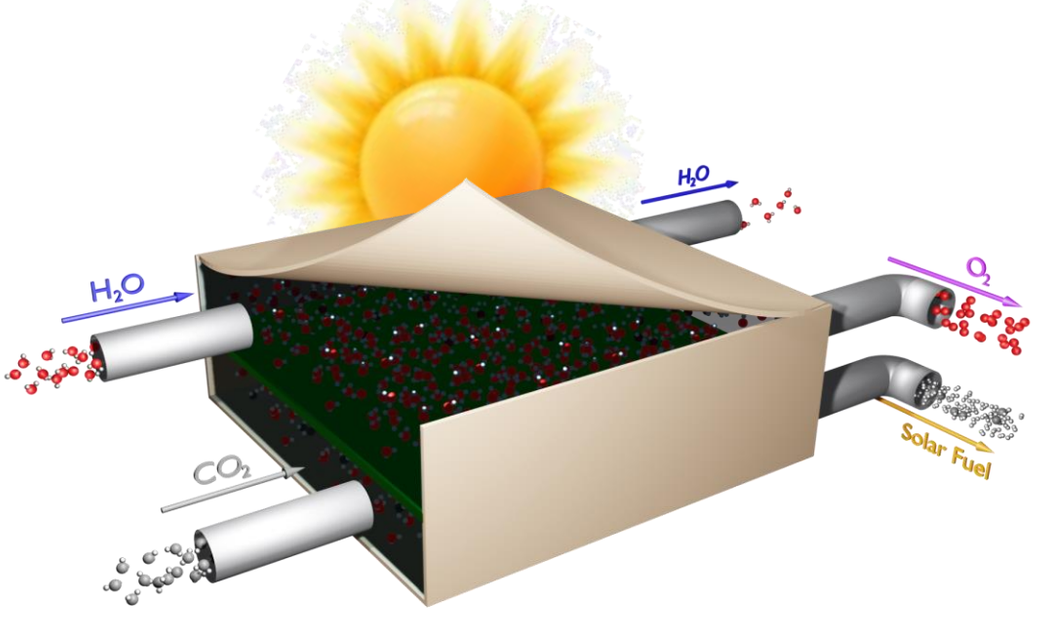

Chapter 1

1

Abstract

In this chapter the development of artificial photosynthesis, especially in dye-sensitized photoelectrochemical (DS-PEC) devices, and the context for this thesis is introduced. In addition, a brief outline of the various computational methods and supporting theories that are used throughout this thesis is presented.

1.1. Introduction

1.1.1 Moving toward Sustainable Energy Sources

With the incremental rise of the global population and rapid development of industrialization and urbanization in the 21st century, the deterioration of environmental and energy crises has been aggravated due to the immoderate usage of non-renewable and carbon-based energy resources such as oil, coal, and natural gas. Currently, approximately 80% of the energy supply worldwide is provided by such fossil fuels, which are closely tied to severe environmental issues, *e.g.*, large quantities of emissions of carbon dioxide (CO_2), sulfur oxide, and other oxide particles, one of the major sources of greenhouse gases for global warming and air pollution.[1] In addition, the global energy consumption has grown at an alarming rate since 2000 without energy innovation to substantially reduce CO_2 emissions, and is predicted to steadily increase to 22 TW in 2030.[2] It is therefore imperative for humankind to search urgently for clean, sustainable, renewable, and environmentally friendly carbon-neutral/carbon-free alternatives of energy sources that have the potential to meet the present and future energy demand in the age of Anthropocene.[3]

Extensive research has been devoted to emerging alternatives such as photovoltaics (PV), dye-sensitized solar cells (DSSC), wind turbines, geothermal energy, tidal energy, and hydroelectric power plants. Renewables are expected to pass the level of 1 TW by 2025 at the latest, mainly due to PV and wind energy, and driven by the emerging economies from China and India. However, the regional dependence, as well as the difficulties and challenges in the storage and transportation of the converted energy in the form of electricity, is considered a hurdle on the way to full large-scale deployment and thus restrict the share of renewables in the future energy markets.[4-5] Since more solar energy provided by the sun is delivered to the surface of the earth every hour than the global energy consumption for a whole year, and it is available almost anywhere, sunlight is considered the most abundant renewable energy source on the planet and to be the ultimate solution for the global energy problem facing humanity.[6-7] Highly efficient conversion of solar energy to other forms of exploitable energy could therefore contribute to the realization of the green earth and a sustainable society. To displace energy carriers from fossil fuels, which are actually stored

sunlight, carbon-free solar fuels storing energy in the form of chemical bonds would be an attractive and practical option.[8]

1.1.2 Natural Photosynthesis

In nature, plants and organisms convert solar energy into chemically accessible energy in the form of chemical bonds via natural photosynthesis by utilizing sunlight, in which molecular oxygen (O_2) and energy-dense carbohydrates (*e.g.*, sugar $C_6H_{12}O_6$) are produced from H_2O and CO_2 through a series of photochemical and chemical reactions, also known as 'Z-scheme' according to the shape of the flow diagram (see Scheme 1.1).[5, 9]

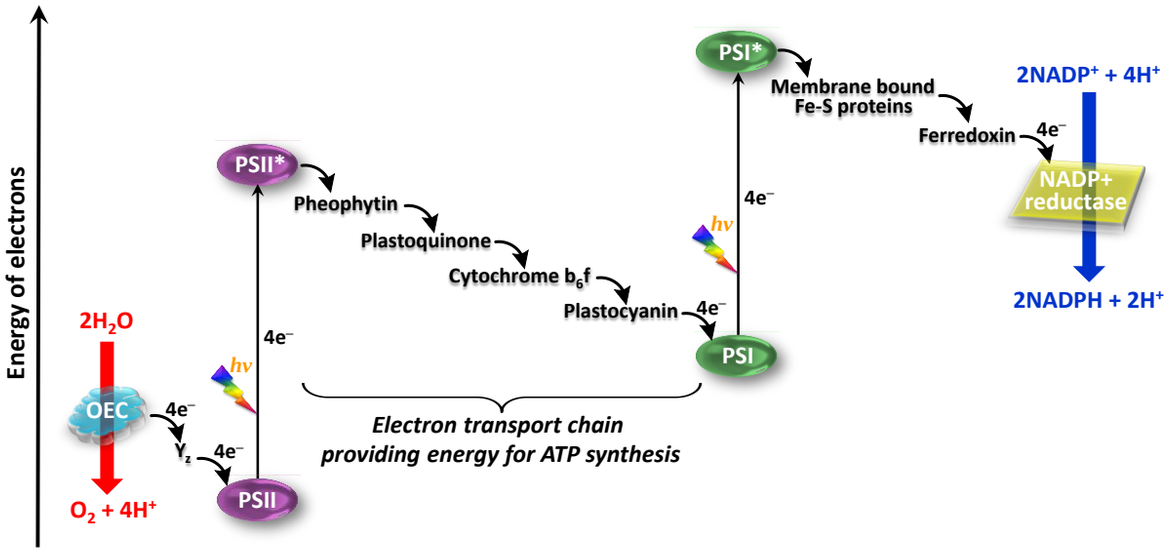

Scheme 1.1. Schematic representation of photosynthesis with the light-absorbing units PSI and PSII, the electron transport chain, the oxygen-evolving center (OEC), and $NADP^+$ reductase. Adapted from Ref. 5 with permission from The Royal Society of Chemistry.

Two coupled cofactor-protein complexes are involved in natural photosynthesis, denoted as photosystem II (PSII) and photosystem I (PSI), respectively (see Scheme 1.1).[10] The absorption of sunlight by chlorophyll P680 (P680 → P680*) of PSII initiates the photosynthesis by pumping electrons to a nearby pheophytin and then to the acceptor side of PSI through rapid electron transfer (ET) steps, generating a charge-separated state (or electron-hole pairs) stable for hundreds of microseconds.[11] The oxidized $P680^+$ provides to the system a necessary driving force to perform redox-reactions and thus activates the photosynthetic water

oxidation and oxygen evolution occurring at the oxygen evolving complex (OEC) of PSII. The OEC consists of a cluster of four manganese ions and a calcium ion (Mn_4Ca). Driven by sunlight, two water molecules are oxidized to form molecular oxygen. Four electrons and protons (H^+) are released by PSII after four light absorption processes (see Scheme 1.1), as shown in eq. 1.1:

$$2H_2O \rightarrow O_2 + 4H^+ + 4e^-. \qquad (1.1)$$

The electrons are transferred to PSI via plastoquinone and cytochrome b_6f molecules to regenerate P700 from the oxidized $P700^+$, the chlorophyll molecules of PSI that are excited and oxidized after capturing a photon. Meanwhile, the reducing power generated by the electron transport chain is used by the ATP synthase complex to drive the conversion of ADP with inorganic phosphorus (P) into ATP. The protons are finally consumed in PSI together with the electrons from the excited P700* for the reduction of $NADP^+$ to NADPH (nicotinamide adenine dinucleotide phosphate).[12-13] The total net reaction for the natural photosynthesis is

$$2H_2O + 2NADP^+ + 3ADP + 3P \rightarrow O_2 + 2H^+ + 2NADPH+ + 3ATP, \qquad (1.2)$$

where the generated NADPH and ATP are subsequently used to fixate atmospheric CO_2 into carbohydrates in the light-independent Calvin-Benson-Bassham cycle.

1.1.3 Artificial Photosynthesis

As a product of mimicking the natural photosynthesis system, artificial photosynthesis has sprung up and attracted dramatically increasing interest in the field of renewable energy production in the past decades.[13-16] The term artificial photosynthesis is commonly used to refer to any human-mediated process that captures and stores solar energy in the chemical bonds of useful and high-enthalpy chemicals, *i.e.* carbohydrates and so-called "solar fuels". Solar energy can be converted either directly into chemical fuels via photoelectrochemical cells (PEC) or indirectly into fuels via PV-electrolysis (PV-E) systems driven by the electricity generated from solar energy (see Figure 1.1).[14, 17] Compared to centralized PV-E, decentralized PEC shows intrinsic advantages since the integration of the PV and electrocatalysis into one device enables it to

operate at low current density, reducing the overpotential and concentration losses.[18] The production of solar fuels and chemicals in artificial photosynthesis has been increasingly investigated since the beginning of the the 21st century, in particular hydrogen production from water splitting, carbon-neutral fuel production from CO_2 reduction, ammonia production from nitrogen fixation, epoxide production from hydrocarbon oxygenation, and hydrogen peroxide production from oxygen reduction.[19-23]

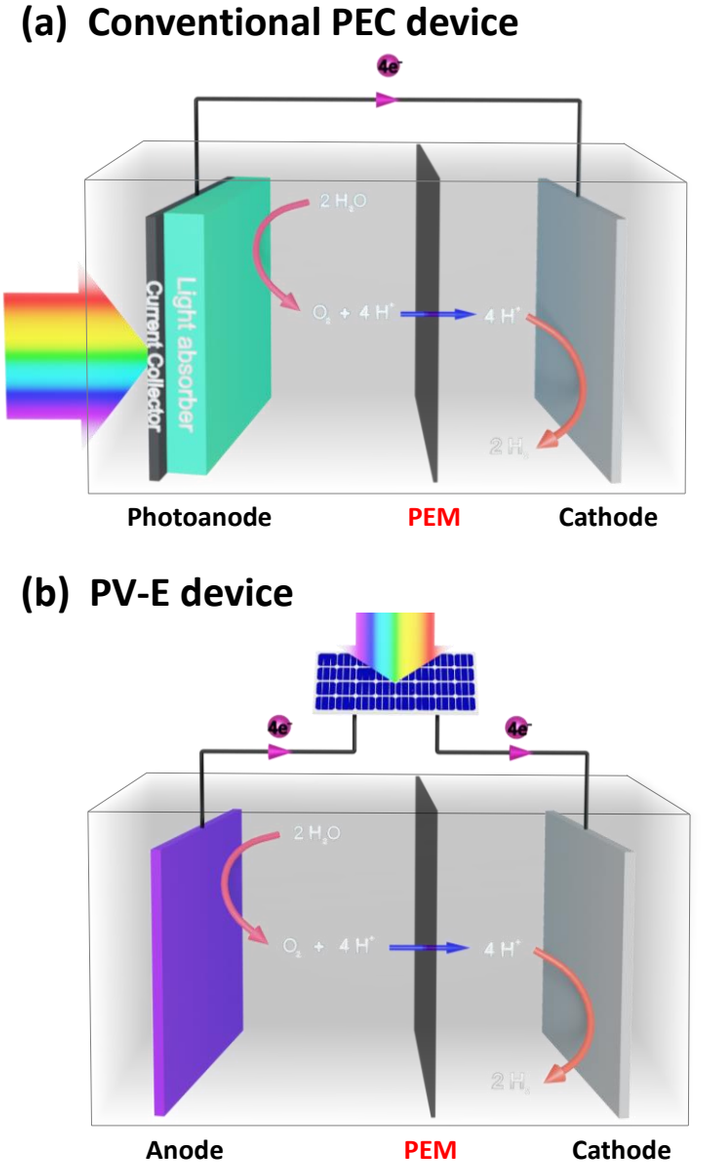

Figure 1.1. Schematic representation of light-driven water electrolysis via artificial photosynthetic systems. (a) Conventional PEC device model; (b) PVE device model. PEM (proton exchange membrane) indicates a proton exchange membrane for selective proton transport to the cathode.

As the smallest and simplest molecule among all the solar fuels, the energy-rich hydrogen (H_2) produces only water (H_2O) as its combustion product and from this perspective it is a most desirable and sustainable energy carrier to fulfill future increasing global energy requirements and to address the environmental pollution issues with zero emission of greenhouse gases.[9] Molecular hydrogen can be derived from a wide variety of feedstocks, especially the cleavage of the abundant resource of water, which covers 70% of the earth. However, the majority of commercial H_2 being used is currently obtained primarily via steam reforming of hydrocarbons with fossil fuels as a feedstock, since H_2 is not readily available in nature. This is costly, complicated, and unsustainable.[24-25] To employ H_2 as a real clean and long-term fuel on a large scale, extensive research effort is still required to develop techniques for the scalable, sustainable, economically viable production of H_2 from renewable sources, such as solar H_2 production by means of direct solar energy conversion from H_2O to storable and transportable carbon-free H_2. In addition, solar-driven CO_2 reduction is also considered as a key process in artificial photosynthesis systems, in which the atmospheric CO_2, one of the predominant greenhouse gases causing global warming and climate change, is fixed to synthesize valuable and sustainable carbon-neutral fuels.

1.1.4 Dye-sensitized Photoelectrochemical cell

Photoelectrochemical water splitting is a promising strategy for direct conversion of solar energy to storable H_2 or CO_2-derived fuels with oxygen as a by-product, providing a sustainable source of renewable energy.[26] A PEC device should in principle combine three key functions governing natural photosynthesis: light harvesting by light absorbers, charge generation and separation in the light absorbers, as well as catalytic water oxidation and reduction.[27] Considerable efforts have been devoted to the development of high-efficiency PEC devices since the pioneering work by Fujishima and Honda in 1972, in which the photoelectrochemical water splitting into H_2 and O_2 was first demonstrated using a rutile TiO_2 semiconductor photoanode coupled with a platinum (Pt) cathode.[28] The use of rutile as photoanode, having a bandgap of 3.0 eV, limits the light absorption to ultraviolet (UV) region, and thus the quantum yield of water splitting under sunlight typically below 2%. Although other visible light-harvesting materials (*e.g.* α-Fe_2O_3[29], WO_3[30], and $BiVO_4$[31]) have been investigated as possible photoanodes, the general drawbacks of them such as

narrow absorption in the solar spectrum, poor hole transport properties, and large bias voltages still need to be improved.[12] One alternative strategy for PEC devices would be to attach molecular photosensitizers onto the surface of the semiconductor anode. Besides, progress in the field is also being challenged by the fundamental understanding of the charge generation and separation processes, as well as the photocatalytic mechanisms, the search for efficient catalysts, *etc*.[15]

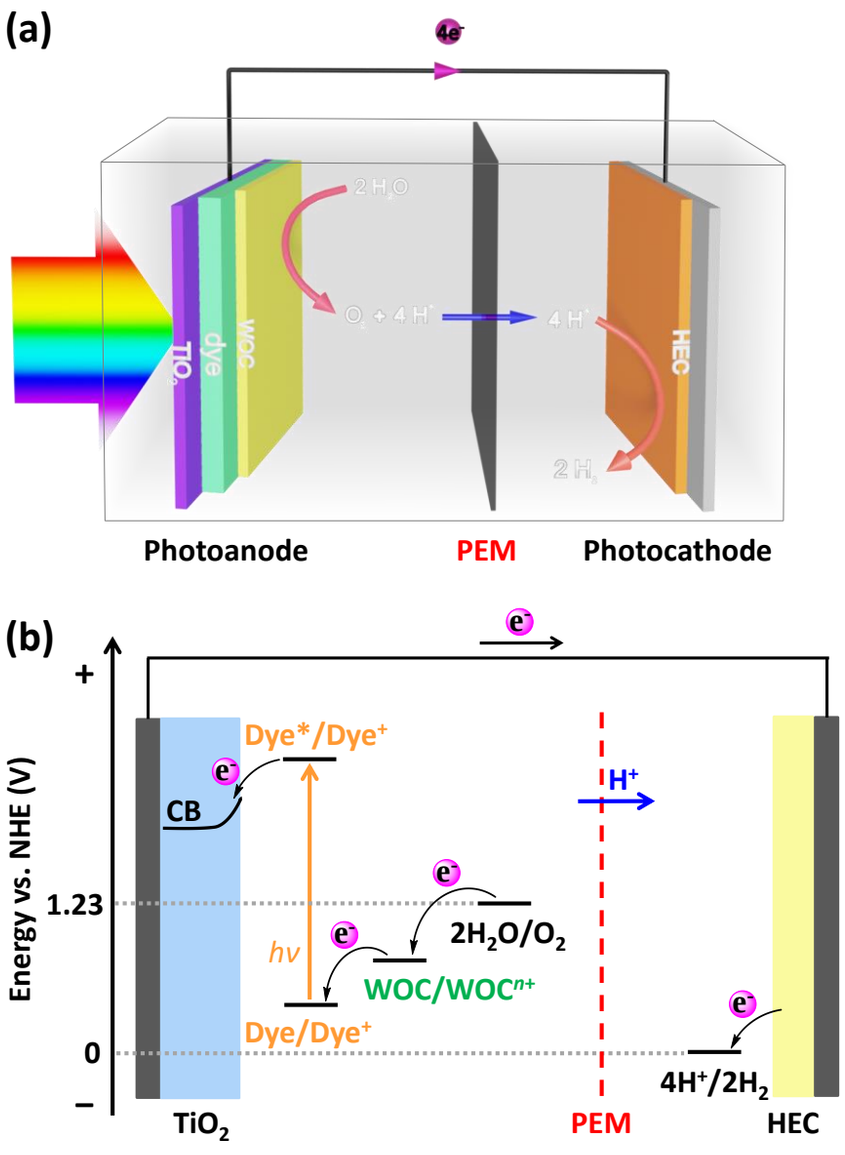

Figure 1.2. (a) Schematic representation of the DS-PEC device model for photocatalytic water splitting. (b) Schematic diagram of a proposed DS-PEC for solar-energy conversion. PEM indicates a proton exchange membrane for selective proton transport to the HEC. CB stands for the conduction band.

Inspired by DSSCs, visible light-harvesting sensitizers are integrated with water oxidation catalysts (WOCs) or hydrogen-evolving catalysts (HECs) on metal-oxide electrodes, thus overcoming the limitations imposed by the band gap of the metal oxide (*e.g.* TiO_2) material. In dye-sensitized PEC (DS-PEC) devices (see Figure 1.2), photons are absorbed in the photoanode, inducing the electron injection from the light-harvesting dye to the metal-oxide semiconductor and thus generating holes on the dye, the so-called charge separation process (see Figure 1.2b). The photo-oxidized dye should provide sufficient driving force for the catalytic multi-electron water oxidation half-reaction and serve as electron acceptor in the catalytic reaction. Under the catalysis of a WOC, water molecules are oxidized to molecular oxygen and protons by the photo-generated holes at the oxidized dye.

The photo-generated electrons migrate through an external circuit or electron-conducting membrane to the (photo)cathode, where protons are consumed for hydrogen production or CO_2 reduction.[9] DS-PECs for solar-driven water splitting provide an opportunity to develop artificial photosynthetic devices in a scalable, affordable and sustainable way for direct solar-to-fuel conversion.

1.1.5 Catalytic water oxidation mechanism

The photocatalytic multi-electron water oxidation half-reaction occurs at the photoanode, requiring a high thermodynamic potential $E^0 \approx 1.23$ V, and has long been considered the most challenging and time-demanding step throughout the entire process limiting the overall yield and large-scale application of DS-PEC devices. In particular, the third catalytic water splitting step involving the O–O bond formation represents a thermodynamic and kinetic bottleneck because of the considerably high activation free energy barrier, especially when considering a single-site catalyst proceeding via a water nucleophilic attack (WNA) mechanism (see Scheme 1.2) partially due to the higher potentials required to produce a sufficiently electrophilic metal–oxo chemical species.[32]

In both natural and artificial photosynthetic systems, the water oxidation proceeds via multiple photo-induced proton-coupled electron transfer (PCET) steps[33-34], which is broadly defined as any process involving the transfer of at least one electron and proton in a single kinetic step. Two general types of mechanisms for these PCET reactions have been widely accepted, either the sequential

mechanism in which the electron transfer and proton transfer (PT) occurs in a stepwise manner (ET first or PT first, see the extended eight-step Kok cycle in Figure 1.3a) or the concerted mechanism in which the movement of both electron and proton occurs simultaneously (also known as concerted electron-proton transfer (EPT)), (see Figure 1.3b).[35] In practice, the distinction between sequential and concerted PCET reactions is normally not rigorous and in part depends on the time scale that one considers. For example, a concerted PCET reaction identified at a long time scale is likely to be decoupled into two-step electron and proton transfer processes within short enough time scales. As a result, these two modes of PCET reactions are often experimentally hard to distinguish one from the other.[36] For the water oxidation in DS-PECs, the overall photocatalytic cycle consists of four PCET steps, which is a greatly uphill reaction requiring the input of energy (Gibbs energy of +237.178 kJ mol^{-1})[12], as depicted in Figure 1.3c showing the pH-independent free energy changes between intermediates along the photocatalytic water splitting cycle.[37] One should bear in mind that a concerted PCET (or EPT) process is normally desirable since it presents a lower energy barrier than that of a sequential PCET reaction. The sequence of these involved electron and proton transfer processes could therefore be fine-tuned to evoke concerted PCET and thus accelerate the catalytic water splitting, which can be achieved by ligand modification[38-42] of WOCs or solvent environmental tuning.[43-46]

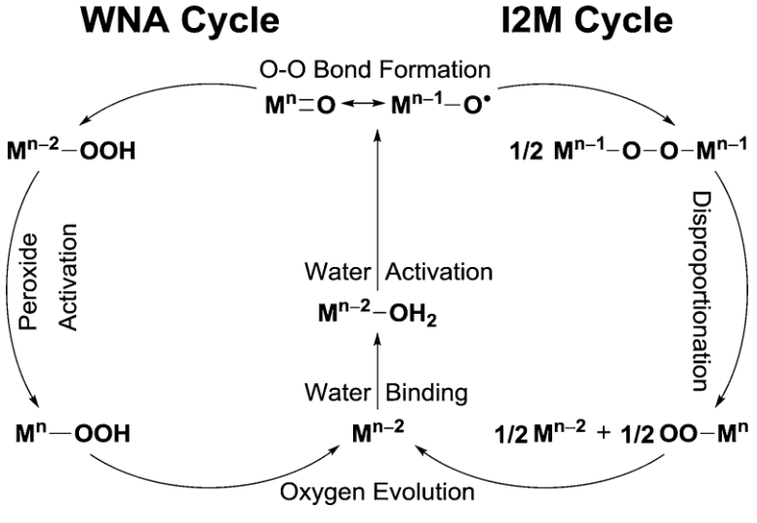

Scheme 1.2. Overview of water nucleophilic attack (WNA) and oxo–oxo coupling (I2M) mechanisms for water oxidation catalysis. Copyright from Ref. 32 with permission from The Royal Society of Chemistry.

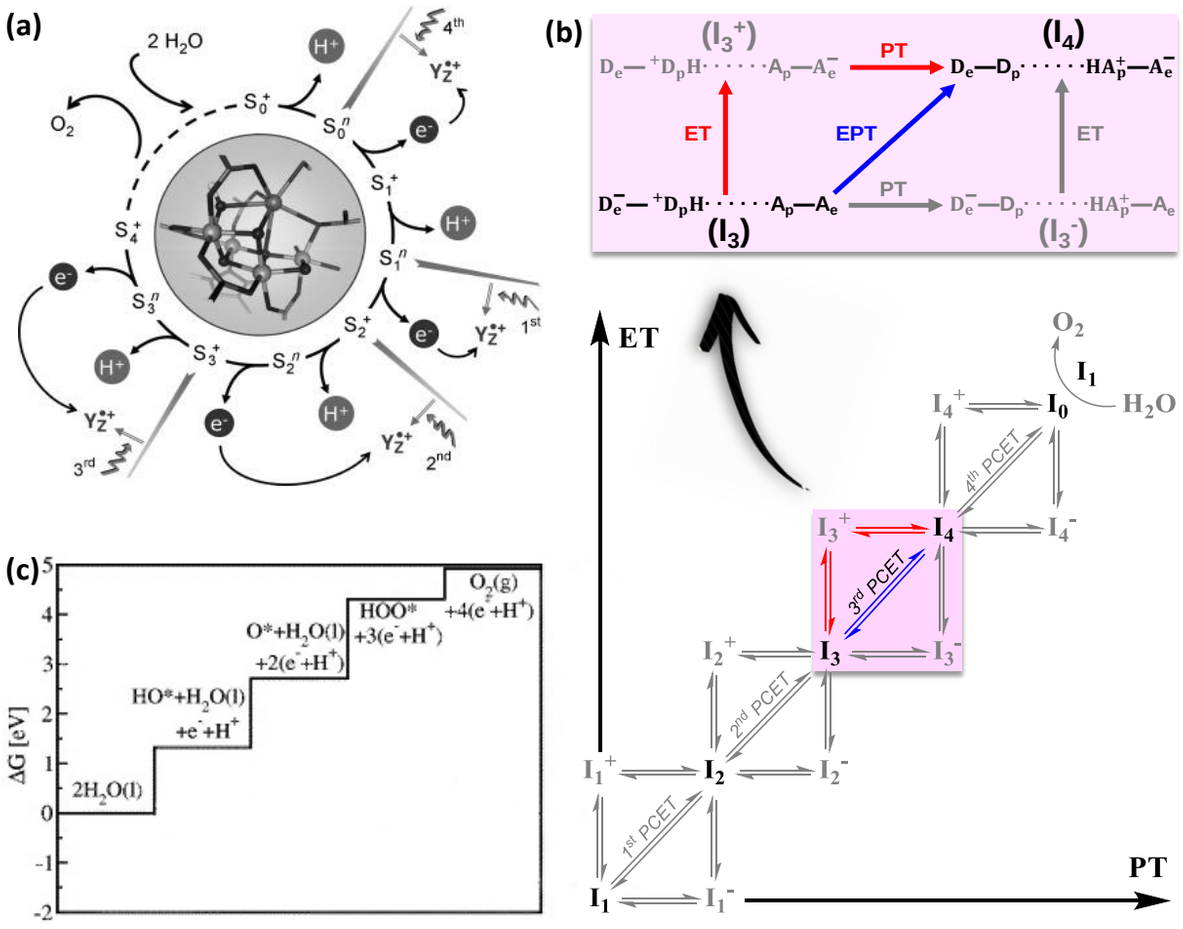

Figure 1.3. (a) Extended Kok's classical *S*-state cycle model including not only four oxidation but also four deprotonation steps by the Mn_4Ca complex in natural systems, as reproduced from Dau et al.[36] In the framework model the coupling between the ET step and the PT step is not covered. (b) The four PCET steps between intermediates (I_i) from I_1 to I_o for water oxidation in a typical DS-PEC device. The vertical and horizontal double arrows correspond to the pathways of sequential mechanisms, either ET first or PT first. The diagonal double arrow denotes the broadly defined PCET and in the top panel the concerted mechanism labeled as EPT (concerted electron-proton tranfer). The stable states are shown in black. The ligand exchange $I_o + H_2O \rightarrow I_1 + O_2$ is also indicated. The third step from I_3 to I_4 is specifically described in the top panel for clarity. The top panel is reproduced with permission from ref. 34. (c) The uphill free energy changes for the four PCET steps by a heterogeneous WOC at an overpotential of η = –1.23 V, where * indicates the adsorbents. Adapted with permission from ref. 37.

In a typical DS-PEC for water splitting, the photoanode combines necessarily two major fundamental components. First, ideal visible light-harvesting photosensitizers exhibit broad absorption in the solar spectrum, have robust anchoring groups to bind to the metal oxide semiconductor surface under aqueous conditions, show high charge carrier mobility, and establish an appropriate redox potential to drive the catalytic water oxidation at a WOC. Second, efficient WOCs modules have high intrinsic activity to overcome the reaction barriers, and show excellent optical and chemical stability, low overpotential, and high reaction rate for catalytic water oxidation. The way these two components are assembled plays a significant role in determining the photostability and efficiency of the DS-PEC device since fast electron transfer between the WOC and the oxidized sensitizer is critical to reducing the charge recombination from the semiconductor surface to the sensitizer and thus increasing the quantum yield.[12] A variety of strategies have been explored for the assembly of DS-PEC devices in the past years, for example, (i) the co-deposition method where the sensitizer and the WOC are deposited as separate moieties on the metal oxide semiconductor surface and (ii) the supramolecular approach where the sensitizer and the WOC are covalently bound forming a complex anchored onto the semiconductor surface.[47-49] In particular, the supramolecular assembly approach by constructing WOC–dye dyads has experimentally and theoretically turned out to be able to facilitate rapid electron transfer from the WOCs to the oxidized sensitizers effectively in homogeneous systems.[9, 50-52] On the other hand, a proper choice of the components in the WOC–dye supramolecular complex in light of the energetics and optical properties of sensitizers and WOCs provides an effective approach to the improvement of a dye-sensitized photoanode as well.[53-55]

Apart from developing novel dinuclear or multinuclear WOCs inspired by the Mn_4Ca complex in natural systems,[36] increasing attention has been focused on mononuclear WOCs since their first appearance in 2005, which breaks the dogma that at least two metal sites are required for catalytic water oxidation.[56-58] The mononuclear complexes serving for water splitting provide guidance in the pursuit of cost-effective and efficient WOCs owing to their common advantages, including simple structures, ease of chemical modification, high catalytic activities, *etc*.[32, 59] In addition, as an equally important component in the dye-sensitized photoanode, the oxidized sensitizer performs the task of stabilizing the

hole and acting as a primary electron acceptor during the catalytic water oxidation cycle, analogous to that of the redox-active tyrosine ($Y_z^{\bullet+}$) near the OEC in PSII (see Figure 1.3a).[36] However, the search for ideal sensitizers is particularly challenging since rare molecules meet all the stringent requirements noted above so far.[12, 60-61] Further optimization of the photoanode design can be achieved by the screening of light-absorbing dyes with excellent optical properties,[62] inclusion of anchoring groups with established chemical and thermal stabilities,[63-65] bridge units with rectifying properties,[66] and ancillary chromophores with complementary absorption properties and redox potentials.[67]

In order to achieve further progress in the field of photoelectrochemical water splitting, computational techniques are and will be increasingly employed in the design and screening of optimal WOCs and sensitizers, in the estimation of the electronic, optical and overall properties of dye-sensitized photoanodes or DS-PEC devices, in the prediction of what happened and what will happen in the real systems that are being studied in response to variable conditions and parameters, in the fundamental understanding and unraveling of the electron transfer processes and catalytic water oxidation mechanisms, as well as in providing additional insights into various engineering problems.[68] The combination of experimental and theoretical approaches has turned out to be necessary to fully understand a given system or process since computational techniques constitute a very useful tool complementary to experiment serving as meaningful touchstones in an easier, reliable and efficient way, which are capable to avoid an expensive trial and error experimental strategy and provide a clear indication on the most cost-effective direction to undertake.[34] The collaboration between experimentalists and theoreticians will be critical for addressing the challenges of demonstrating photocatalytic water splitting at a near-unity yield.

Despite all the efforts in the development of novel DS-PEC devices with improved photoelectrodes[69-70] or ion-exchange membranes[71-72], the overall yield of the water oxidation half-reaction is still low, normally less than 20%.[73] Nevertheless, the motivation and determination for developing and optimizing high-performance artificial photosynthetic devices have remained and the work on artificial photosynthesis, especially concerning DS-PEC devices, is continuing to promote the realization of the green earth and sustainable society from the blueprint to reality.

Chapter 1

1.2. Computational Tools

1.2.1 Density Functional Theory (DFT)

Considering that the nuclei are much heavier than the electrons in mass (about 2000 times), the nuclei move on much longer timescales than the electrons, allowing the electrons to respond almost instantaneously to the motion of the nuclei. In light of this fact, the Born-Oppenheimer (BO) approximation has been proposed in the early period of quantum mechanics, in which the electronic motion and the nuclear motion in molecules are treated separately, thus facilitating the description of the quantum states of molecules.[74] More precisely, in the BO approximation the motion of the atomic nuclei is neglected, *i.e.* the nuclei are assumed to be fixed at given positions when describing the electrons in a molecule. On this basis, the electronic structure (ground state and excited states) of given systems can be determined by solving the electronic Schrödinger equation as a function of the nuclear coordinates.

With the goal of simulating the behavior of atomic and molecular systems, density functional theory (DFT) has been widely used as one of the most popular and successful computational quantum mechanical approaches for *ab initio* calculations of the structural and dynamical properties of many-body systems. As Kohn noted in his Nobel lecture, DFT "has been most useful for systems of very many electrons where wave function methods encounter and are stopped by the "exponential wall".[75] At variance from Hartree-Fock and multi-configuration theories that deal directly with the many-body wavefunction, in DFT the electronic energy of the system can be obtained as a functional of the electron density $\rho(\mathbf{r})$, which is defined as the average number of electrons per unit volume. The use of the electron density in obtaining an approximate solution to the Schrödinger equation and therefore describing the complicated physics behind the many-body electronic interactions, makes DFT computationally less expensive than wave function methods and yet sufficiently accurate.

At the heart of DFT, the Hohenberg-Kohn theorem states that the electron density determines all ground-state properties of the system, indicating the total energy of a many-body system as a functional of the ground-state density.[76]

According to the form of the electronic Schrödinger equation, the energy functional of a many-electron interacting system can be written as

$$E[\rho] = T[\rho] + V_{\text{ext}}[\rho] + V_{\text{ee}}[\rho], \tag{1.3}$$

where the functional of the nucleus-electron interaction $V_{\text{ext}}[\rho]$ is explicitly known. It can be expressed in terms of a general external potential $v_{\text{ext}}(\mathbf{r})$ created either by the electrostatic field of the nuclei or external electric fields applied to the system

$$V_{\text{ext}}[\rho] = \int \rho(\mathbf{r}) v_{\text{ext}}(\mathbf{r}) \mathrm{d}^3\mathbf{r}. \tag{1.4}$$

Unfortunately, the other two energy components, the kinetic energy functional $T[\rho]$, and the electron-electron interaction functional $V_{\text{ee}}[\rho]$, are unknown. In order to realize the direct minimization of the energy, proper approximations to these unknown terms are necessary.

In Kohn-Sham (KS) theory,[77] a fictitious system of N non-interacting electrons was proposed, in which a single determinant wavefunction in N "orbitals" $\{\phi_i\}$ was introduced to describe the N non-interacting electrons. These KS orbitals $\{\phi_i\}$ can be used to obtain the electron density of the KS non-interacting system

$$\rho(\mathbf{r}) = \sum_{i}^{\mathrm{N}} |\phi_i(\mathbf{r})|^2 \tag{1.5}$$

in atomic units, in which the Coulomb's constant, electron mass, elementary charge and the reduced Planck's constant are defined to be 1. The kinetic energy for the many-body system is expressed in terms of $\{\phi_i\}$ according to

$$\begin{aligned} T[\rho] &= T_{\text{s}}[\rho] + T_{\text{c}}[\rho] \\ &= -\frac{1}{2}\sum_{i}^{\mathrm{N}} \langle \phi_i | \nabla^2 | \phi_i \rangle + T_c[\rho], \end{aligned} \tag{1.6}$$

where $T_{\text{s}}[\rho]$ is the kinetic energy of the KS non-interacting reference system and the kinetic correlation energy $T_{\text{c}}[\rho]$ indicates the remaining unknown part of the kinetic energy for the actual interacting many-body system.

Considering that the classical Coulomb interaction $J[\rho]$ accounts for a significant component of the electron-electron interaction $V_{\text{ee}}[\rho]$ in many-body systems, the total

$V_{ee}[\rho]$ can be expressed as the sum of two parts, the known classical Coulomb interaction $J[\rho]$ and the unknown non-classical part $V_{nc}[\rho]$ integrated over all space

$$\begin{aligned} V_{ee}[\rho] &= J[\rho] + V_{nc}[\rho] \\ &= \frac{1}{2}\iint \frac{\rho(\mathbf{r})\rho(\mathbf{r}')}{|\mathbf{r}-\mathbf{r}'|}\mathrm{d}\mathbf{r}\mathrm{d}\mathbf{r}' + V_{nc}[\rho] \end{aligned} \tag{1.7}$$

The ground state energy of the many-body system is then formulated as

$$\begin{aligned} E[\rho] &= T[\rho] + V_{ext}[\rho] + V_{ee}[\rho] \\ &= (T_s[\rho] + T_c[\rho]) + V_{ext}[\rho] + (J[\rho] + V_{nc}[\rho]) \\ &= T_s[\rho] + V_{ext}[\rho] + J[\rho] + (T_c[\rho] + V_{nc}[\rho]) \\ &= T_s[\rho] + V_{ext}[\rho] + J[\rho] + E_{xc}[\rho], \end{aligned} \tag{1.8}$$

where the exchange-correlation functional $E_{xc}[\rho]$ is introduced to represent the total error made in using non-interacting kinetic energy and in treating the electron-electron interaction classically.

With a given approximation for the $E_{xc}[\rho]$, the minimization of the energy functional leads to the KS equations

$$\left[-\frac{1}{2}\nabla^2 + v_{ext}(\mathbf{r}) + \int \frac{\rho(\mathbf{r}')}{|\mathbf{r}-\mathbf{r}'|}\mathrm{d}\mathbf{r}' + v_{xc}(\mathbf{r})\right]\phi_i(\mathbf{r}) = \varepsilon_i\phi_i(\mathbf{r}), \tag{1.9}$$

where the local exchange-correlation potential $v_{xc}(\mathbf{r})$ is the functional derivative of the exchange-correlation functional with respect to the density

$$v_{xc}(\mathbf{r}) = \frac{\delta E_{xc}[\rho]}{\delta\rho}. \tag{1.10}$$

The self-consistent-field solution of the KS equations provides the ground state energy, which depends on the given/approximated $E_{xc}[\rho]$ functional.

Although there is still no explicit form available for the key exchange-correlation functional $E_{xc}[\rho]$, luckily $E_{xc}[\rho]$ is in general energetically substantially smaller than any other known terms, theoretically allowing for reasonable simple approximations of $E_{xc}[\rho]$ to obtain accurate estimates of the ground-state many-body energy.

1.2.2 Exchange-Correlation Functionals and Other Approximations

In the search for an exact formulation for density functionals, $E_{xc}[\rho]$ can be expressed as

$$\begin{aligned} E_{xc}(\rho) &= \min_{\Psi\to\rho}\langle\Psi|T+V_{ee}|\Psi\rangle - T_s[\rho] - J[\rho] \\ &= (T[\rho]-T_s[\rho]) + (V_{ee}[\rho]-J[\rho]). \end{aligned} \tag{1.11}$$

To develop accurate exchange-correlation functionals for DFT, the form of $E_{xc}[\rho]$ has to be approximated in a sufficiently precise way for different applications, which will determine the level of accuracy of the DFT results. With this goal, a variety of density functional approximations have been proposed, leading to great improvements in practical expressions for $E_{xc}[\rho]$, such as the local density approximation (LDA), the gradient expansion approximation (GEA), the generalized gradient approximation (GGA), and the Hybrid Exchange Functionals.[78]

In particular, the introduction of the first derivative of the density in GGA leads to an energy functional that depends not only on the density but also on the gradient of the density, taking into account as well the non-homogeneity of the true electron density, and then initially enables the satisfactory application of DFT in the chemistry community. The general form for a GGA functional is

$$E_{xc}^{GGA}[\rho,\nabla\rho] = \int \rho(\mathbf{r})v_{xc}\big(\rho(\mathbf{r}),\nabla\rho(\mathbf{r})\big)\,d\mathbf{r}. \tag{1.12}$$

As one of the best-performing GGA functionals, OPBE,[79] which combines Handy's optimized exchange (OPTX) with the PBE correlation, is primarily used in this thesis since the OPBE functional has shown to be able to accurately describe the transition-metal complexes, especially regarding the prediction of spin states.

In DFT, molecular orbitals are usually expanded as a linear combination of basis functions, most often atomic-like orbitals. However, when dealing with periodic systems, an alternative basis set consists of plane waves within a chosen cut-off energy. The choice of the basis set determines the level of accuracy and efficiency in DFT calculations. In the ADF (Amsterdam Density Functional software package[80-81]) calculations, the Slater-type basis set, all-electron TZP (triple-ζ

polarized), is used for the considered systems, which provides an excellent balance between the accuracy of the results and the computational cost.

To further improve the computational efficiency of DFT-based calculations, pseudopotentials have been proposed to dramatically simplify the electronic structure calculations and thus save valuable computing time by replacing the core (*i.e.* non-valence) electrons and the strong nuclear potential with a softer potential (or pseudopotential) in a reliable way. Furthermore, the use of pseudopotentials in conjunction with a plane-wave basis set is a commonly used approach in electronic structure calculations. Specifically, the Car-Parrinello Molecular Dynamics program[82] (CPMD) extensively used in this thesis, makes use of the plane wave/pseudopotential implementation of DFT, with pseudopotentials in the separable (Kleinman-Bylander) form.[83-84]

Additionally, considering that the van der Waals interactions play a significant role in most chemical systems, dispersion corrections developed by Grimme are also added to account for the effect of van der Waals forces in the systems.[85]

1.2.3 Car-Parrinello Molecular Dynamics (CPMD)

Molecular dynamics (MD) is a powerful technique to investigate the real-time evolution of a system of interacting particles and thus to analyze equilibrium thermodynamic and dynamic properties of rather complex many-body systems at an atomistic level of description. In MD simulations the trajectories of atoms and molecules are governed by classical mechanics and Newton's laws of motion are used to predict the spatial position of each atom in the system as a function of time. Electrons are not present explicitly in MD simulations and the forces exerted on each atom are computed from molecular mechanics force fields comprised of empirical parameters, which are fitted to available experimental data or to results of quantum mechanical calculations. The simplified description of interatomic interaction and atomic motion, the poor transferability of force-fields, together with the insufficient predictive power in simulating chemical bonding processes are severe limitations of classical MD methods to provide a realistic quantitative analysis of the behavior and properties of real systems, especially when dealing with chemical reactions. Therefore, attractive approaches based on first principles are desirable to remove these limitations, such as in *ab initio* molecular dynamics (AIMD). However, AIMD simulations to increase the

accuracy and predictive power normally come at a significant computational cost because of the need to solve the electronic problem to compute atomic forces.

The CPMD approach, introduced by Car and Parrinello in 1985,[86-87] is an extremely efficient implementation of AIMD. While in the straightforward Born-Oppenheimer Molecular Dynamics (BOMD) method explicit minimization of the electronic density functional is required at each time step, in CPMD this is done only for the initial nuclear configuration. In CPMD, a fictitious Newtonian dynamics is introduced for the electronic variables that keeps the electrons on the electronic ground state corresponding to each instantaneous ionic configuration, leading to a system of coupled electron-ion dynamics. More specifically, the electronic structure is only minimized for the initial configuration in CPMD simulations and then evolved in time using an extended Lagrangian formulation, which in turn provides accurate forces to drive the nuclear dynamics. The Euler-Lagrange equations of motion resulting from the Lagrangian are

$$M_{\mathrm{I}} \frac{d^2}{dt^2} \mathbf{R}_I = -\nabla_I E[\{\phi_i\}, \mathbf{R}_I] \tag{1.13}$$

and

$$\mu \frac{d^2}{dt^2} \phi_i(\mathbf{r}, t) = -\frac{\delta E}{\delta \phi_i^*(\mathbf{r}, t)} + \sum_j \Lambda_{ij} \phi_j(\mathbf{r}, t) \tag{1.14}$$

for the dynamics of the nuclei with mass M and the evolution of the electrons respectively, where μ is the fictitious mass of the electronic degrees of freedom, Λ_{ij} the Lagrange multipliers associated to the orthonormalization condition of the KS orbitals ϕ_i, and E the energy functional as expressed in equation 1.8.

With such an algorithm, the computational cost of CPMD simulations is significantly lowered owing to the simultaneous calculation of the nuclear trajectory and corresponding instantaneous electronic ground state, thus allowing the dynamical investigation of relatively large systems (several hundred atoms) for a time scale of the order of ~10 ps in practical applications. Although in principle AIMD can be used in conjunction with any electronic structure method, DFT is most commonly employed to solve the electronic problems with the advantage of highly balanced accuracy and computing time.

Chapter 1

1.2.4 Free Energy Calculations

Activated processes, such as the PCET steps in artificial photosynthetic water splitting, are customarily regarded as rare events occurring with low frequency. In these processes a transition occurs between two stable states, the initial state (IS) and final state (FS), separated by an activation free energy barrier (ΔG^*), which is the free energy change from the initial state of stable reactants to the transition state (TS). If the activation free energy barrier is very high compared to the thermal energy $k_B T$, the reaction is very unlikely to proceed spontaneously within the typical MD simulation time scale, which therefore leads to a low probability to locate the system close to the transition state.

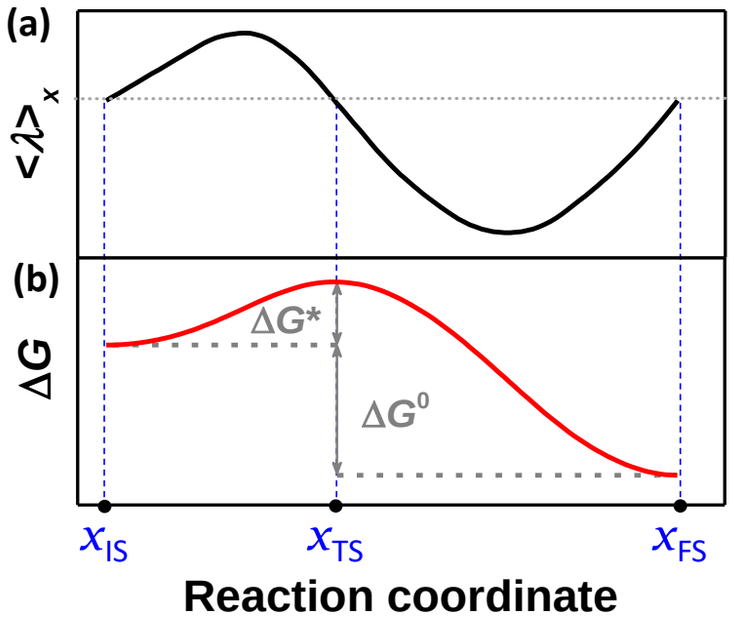

Figure 1.4 (a) Time-averaged constraint force represented by the Lagrangian multiplier $\langle\lambda\rangle_x$ as a function of the reaction coordinate x. (b) Free energy profile along the reaction coordinate computed from thermodynamic integration. ΔG^o represents the thermodynamic driving force.

The "bottleneck" regions of the phase space would be rarely reached during a DFT-based Car-Parrinello MD (DFT-MD) simulation. The so-called Blue Moon approach,[88] is a constrained MD method,[89-90] and is employed in this thesis to compute the free energy profile along the photocatalytic water oxidation reaction consisting of four PCET steps. Particular attention is devoted to the third PCET

step involving the O–O bond formation process. To do so, the reaction coordinate, a function of the positions of the nuclei (in this thesis the distance between two atoms), is constrained to a series of fixed values in the range of $x_{IS} < x < x_{FS}$ along a certain reaction path, where x_{IS} corresponds to the reaction coordinate at the initial state and x_{FS} the reaction coordinate at the final state. For each value of the reaction coordinate x a time-averaged constraint force (or mean force) $<\lambda>_x$ is obtained, where λ is the Lagrangian multiplier associated to the constraint at x. This time-averaged constraint force should be equal to zero at an equilibrium or transition state, *i.e.*, $\langle\lambda\rangle_{x_{IS}} = 0$, $\langle\lambda\rangle_{x_{TS}} = 0$, and $\langle\lambda\rangle_{x_{FS}} = 0$ (see Figure 1.4). The free energy change for each catalytic step is then obtained by thermodynamic integration of the time-averaged constraint force along the reaction path

$$\Delta G(x) = \int_{x_{IS}}^{x_{FS}} \langle\lambda\rangle_x \mathrm{d}x. \tag{1.15}$$

According to standard transition state theory,[91-92] the reaction rate (k) determined by the activation free energy barrier ΔG^* can be expressed as

$$k = \frac{k_B T}{h} \cdot e^{-\frac{\Delta G^*}{RT}}, \tag{1.16}$$

where R and T are the universal gas constant and thermodynamic temperature, respectively. One should keep in mind that in the DFT-MD simulations protons are treated classically and thus proton tunneling effects are neglected. In the current study, only the activation energy barrier is considered as the main factor governing the reaction rate.

1.3. Aim and Outline of This Thesis

PCET plays a crucial role in a wide range of biological and chemical reactions concerning energy conversion processes, such as natural and artificial photosynthesis. Given that the overall catalytic water oxidation consists of four consecutive PCET steps, sequential or concerted, it is therefore of fundamental significance to unveil the intrinsic catalytic mechanism as well as the factors determining the PCET rate and thus to find strategies to facilitate the catalytic water oxidation. Computational tools provide a powerful and essential technique

for the understanding and engineering of efficient DS-PEC devices for water splitting.

In Chapter 2, constrained AIMD simulations are performed to explore the photocatalytic water splitting cycle driven by a supramolecular WOC–dye complex integrating a mononuclear Ru-based WOC with a fully organic naphthalene-diimide (NDI) dye in explicit water solvent and to estimate the free energy profile for each catalytic step. The proton and electron dynamics are followed to demonstrate the effect of spin alignment and solvent rearrangement in facilitating the PCET processes.

Since the O–O bond formation process via water nucleophilic attack has been confirmed to be the thermodynamic and kinetic bottleneck in photocatalytic water oxidation due to the considerably high activation free energy barrier, in Chapter 3 a proton acceptor group (OH^-) is introduced in the hydration shell near the catalytic active site to investigate how and to what extent the solvent tuning, in this case the introduction of an extra proton acceptor, can accelerate the O–O bond formation process in a WOC–dye supramolecular complex by means of CPMD simulations.

Recent analysis of PCET reactions acknowledges the importance of nonadiabatic terms connecting electronic states, which are usually treated as probabilistic events for the conversion of reactants into products in the context of nonadiabatic transition state theory.[34, 93] Constrained AIMD simulations are carried out to investigate the rate-limiting step in catalytic water oxidation in a series of WOC–dye supramolecular complexes functionalized with different alkyl groups on the catalyst component to understand if and how the resonant coupling between electronic and nuclear motions can accelerate the PCET rate in the O–O bond formation process in Chapter 4.

In Chapter 5, a two-channel model for ET in a dye–WOC–dye supramolecular complex is proposed for photocatalytic water splitting, in which a Ru-based WOC is covalently bonded to two NDI dyes. The two-channel model with two separate electron-transfer channels is investigated by constrained AIMD simulations to estimate the probability of the concurrent ET event from the WOC to the two separate dyes and to explore the possible intermediates involved and the sequence of ET/PT/PCET events along the photocatalytic water splitting cycle.

1.4. References

[1] Purchase, R. L.; de Groot, H. J. M. *Interface Focus* **2015,** *5*, 20150014.
[2] Hisatomi, T.; Domen, K. *Faraday Discuss.* **2017,** *198*, 11-35.
[3] Pinaud, B. A.; Benck, J. D.; Seitz, L. C.; Forman, A. J.; Chen, Z.; Deutsch, T. G.; James, B. D.; Baum, K. N.; Baum, G. N.; Ardo, S.; Wang, H.; Miller, E.; Jaramillo, T. F. *Energy Environ. Sci.* **2013,** *6*, 1983-2002.
[4] Lewis, N. S.; Nocera, D. G. *Proc. Natl. Acad. Sci.* **2006,** *103*, 15729-15735.
[5] Berardi, S.; Drouet, S.; Francas, L.; Gimbert-Surinach, C.; Guttentag, M.; Richmond, C.; Stoll, T.; Llobet, A. *Chem. Soc. Rev.* **2014,** *43*, 7501-7519.
[6] Kärkäs, M. D.; Verho, O.; Johnston, E. V.; Åkermark, B. *Chem. Rev.* **2014,** *114*, 11863-12001.
[7] Chu, S.; Li, W.; Yan, Y.; Hamann, T.; Shih, I.; Wang, D.; Mi, Z. *Nano Futures* **2017,** *1*, 022001.
[8] Ronge, J.; Bosserez, T.; Martel, D.; Nervi, C.; Boarino, L.; Taulelle, F.; Decher, G.; Bordiga, S.; Martens, J. A. *Chem. Soc. Rev.* **2014,** *43*, 7963-7981.
[9] Yu, Z.; Li, F.; Sun, L. *Energy Environ. Sci.* **2015,** *8*, 760-775.
[10] Dau, H.; Zaharieva, I. *Acc. Chem. Res.* **2009,** *42*, 1861-1870.
[11] de Wijn, R.; van Gorkom, H. J. *Biochim. Biophys. Acta, Bioenerg.* **2002,** *1553*, 302-308.
[12] Swierk, J. R.; Mallouk, T. E. *Chem. Soc. Rev.* **2013,** *42*, 2357-2387.
[13] Cox, N.; Pantazis, D. A.; Neese, F.; Lubitz, W. *Interface Focus* **2015,** *5*, 20150009.
[14] Zhang, B.; Sun, L. *Chem. Soc. Rev.* **2019,** *48*, 2216-2264.
[15] Bozal-Ginesta, C.; Durrant, J. R. *Faraday Discuss.***2019,** *215*, 439-451.
[16] Ye, S.; Ding, C.; Liu, M.; Wang, A.; Huang, Q.; Li, C. *Adv. Mater.* **2019,** *31*, 1902069.
[17] Jacobsson, T. J.; Fjallstrom, V.; Edoff, M.; Edvinsson, T. *Energy Environ. Sci.* **2014,** *7*, 2056-2070.
[18] Purchase, R.; Cogdell, R.; Breitling, F.; Stadler, V.; Hulst, N. v.; Kramer, G.-J.; Ramirez, A.; Zwijnenberg, R.; Kallergi, A.; Baan, J. B. d.; Rudra, I.; de Groot, H. J. M. Semi-Synthetic Responsive Matrices for Artificial Photosynthesis, *In Series on Chemistry, Energy and the Environment*, (Eds.: K. M., Kadish, R. Gullard), World Scientific, **2019**; pp. 47–69.
[19] Ardo, S.; Fernandez Rivas, D.; Modestino, M. A.; Schulze Greiving, V.; Abdi, F. F.; Alarcon Llado, E.; Artero, V.; Ayers, K.; Battaglia, C.; Becker, J.-P.; Bederak, D.; Berger, A.; Buda, F.; Chinello, E.; Dam, B.; Di Palma, V.; Edvinsson, T.; Fujii, K.; Gardeniers, H.; Geerlings, H.; H. Hashemi, S. M.; Haussener, S.; Houle, F.; Huskens, J.; James, B. D.; Konrad, K.; Kudo, A.; Kunturu, P. P.; Lohse, D.; Mei, B.; Miller, E. L.; Moore, G. F.; Muller, J.; Orchard, K. L.; Rosser, T. E.; Saadi, F. H.; Schüttauf, J.-W.; Seger, B.; Sheehan, S. W.; Smith, W. A.; Spurgeon, J.; Tang, M. H.; van de Krol, R.; Vesborg, P. C. K.; Westerik, P., *Energy Environ. Sci.* **2018**, *11*, 2768-2783.
[20] Shaner, M. R.; Atwater, H. A.; Lewis, N. S.; McFarland, E. W. *Energy Environ. Sci.* **2016,** *9*, 2354-2371.
[21] Jia, J.; Seitz, L. C.; Benck, J. D.; Huo, Y.; Chen, Y.; Ng, J. W. D.; Bilir, T.; Harris, J. S.; Jaramillo, T. F. *Nat. Commun.* **2016,** *7*, 13237.
[22] Gutierrez, R. R.; Haussener, S. *J. Electrochem. Soc.* **2016,** *163*, H1008-H1018.
[23] Haas, T.; Krause, R.; Weber, R.; Demler, M.; Schmid, G. *Nat. Catal.* **2018,** *1*, 32-39.
[24] Abdalla, A. M.; Hossain, S.; Nisfindy, O. B.; Azad, A. T.; Dawood, M.; Azad, A. K. *Energy Convers. Manage.* **2018,** *165*, 602-627.
[25] Gibson, E. A. *Chem. Soc. Rev.* **2017,** *46*, 6194-6209.
[26] Grätzel, M. *Nature* **2001,** *414*, 338-344.
[27] Monti, A.; de Ruiter, J. M.; de Groot, H. J. M.; Buda, F. *J. Phys. Chem. C* **2016,** *120*, 23074-23082.
[28] Fujishima, A.; Honda, K. *Nature* **1972,** *238*, 37-38.
[29] Sivula, K.; Le Formal, F.; Grätzel, M. *ChemSusChem* **2011,** *4*, 432-449.
[30] Kalanur, S. S.; Duy, L. T.; Seo, H. *Top. Catal.* **2018,** *61*, 1043-1076.

[31] Park, Y.; McDonald, K. J.; Choi, K.-S. *Chem. Soc. Rev.* **2013,** *42*, 2321-2337.
[32] Shaffer, D. W.; Xie, Y.; Concepcion, J. J. *Chem. Soc. Rev.* **2017,** *46*, 6170-6193.
[33] Hammes-Schiffer, S. *Chem. Rev.* **2010,** *110*, 6937-6938.
[34] Hammes-Schiffer, S. *J. Am. Chem. Soc.* **2015,** *137*, 8860-8871.
[35] Hammes-Schiffer, S. *Energy Environ. Sci.* **2012,** *5*, 7696-7703.
[36] Dau, H.; Limberg, C.; Reier, T.; Risch, M.; Roggan, S.; Strasser, P. *ChemCatChem* **2010,** *2*, 724-761.
[37] Rossmeisl, J.; Qu, Z. W.; Zhu, H.; Kroes, G. J.; Nørskov, J. K. *J. Electroanal. Chem.* **2007,** *607*, 83-89.
[38] Maji, S.; Vigara, L.; Cottone, F.; Bozoglian, F.; Benet-Buchholz, J.; Llobet, A. *Angew. Chem. Int. Ed.* **2012,** *51*, 5967-5970.
[39] Garrido-Barros, P.; Funes-Ardoiz, I.; Drouet, S.; Benet-Buchholz, J.; Maseras, F.; Llobet, A. *J. Am. Chem. Soc.* **2015,** *137*, 6758-6761.
[40] Wilson, A. D.; Newell, R. H.; McNevin, M. J.; Muckerman, J. T.; Rakowski DuBois, M.; DuBois, D. L. *J. Am. Chem. Soc.* **2006,** *128*, 358-366.
[41] Bediako, D. K.; Solis, B. H.; Dogutan, D. K.; Roubelakis, M. M.; Maher, A. G.; Lee, C. H.; Chambers, M. B.; Hammes-Schiffer, S.; Nocera, D. G. *Proc. Natl. Acad. Sci.* **2014,** *111*, 15001-15006.
[42] Solis, B. H.; Maher, A. G.; Honda, T.; Powers, D. C.; Nocera, D. G.; Hammes-Schiffer, S. *ACS Catal.* **2014,** *4*, 4516-4526.
[43] Song, N.; Concepcion, J. J.; Binstead, R. A.; Rudd, J. A.; Vannucci, A. K.; Dares, C. J.; Coggins, M. K.; Meyer, T. J. *Proc. Natl. Acad. Sci.* **2015,** *112*, 4935-4940.
[44] Coggins, M. K.; Zhang, M.-T.; Chen, Z.; Song, N.; Meyer, T. J. *Angew. Chem. Int. Ed.***2014,** *53*, 12226-12230.
[45] Chen, Z.; Concepcion, J. J.; Song, N.; Meyer, T. J. *Chem. Commun.* **2014,** *50*, 8053-8056.
[46] Stewart, D. J.; Concepcion, J. J.; Brennaman, M. K.; Binstead, R. A.; Meyer, T. J. *Proc. Natl. Acad. Sci.* **2013,** *110*, 876-880.
[47] Ding, X.; Gao, Y.; Ye, L.; Zhang, L.; Sun, L. *ChemSusChem* **2015,** *8*, 3992-3995.
[48] Moore, G. F.; Blakemore, J. D.; Milot, R. L.; Hull, J. F.; Song, H.-e.; Cai, L.; Schmuttenmaer, C. A.; Crabtree, R. H.; Brudvig, G. W. *Energy Environ. Sci.* **2011,** *4*, 2389-2392.
[49] Ji, Z.; He, M.; Huang, Z.; Ozkan, U.; Wu, Y. *J. Am. Chem. Soc.* **2013,** *135*, 11696-11699.
[50] Li, F.; Jiang, Y.; Zhang, B.; Huang, F.; Gao, Y.; Sun, L. *Angew. Chem. Int. Ed.***2012,** *51*, 2417-2420.
[51] Vagnini, M. T.; Smeigh, A. L.; Blakemore, J. D.; Eaton, S. W.; Schley, N. D.; D'Souza, F.; Crabtree, R. H.; Brudvig, G. W.; Co, D. T.; Wasielewski, M. R. *Proc. Natl. Acad. Sci.* **2012,** *109*, 15651-15656.
[52] Frischmann, P. D.; Mahata, K.; Würthner, F. *Chem. Soc. Rev.* **2013,** *42*, 1847-1870.
[53] Luo, J.; Im, J.-H.; Mayer, M. T.; Schreier, M.; Nazeeruddin, M. K.; Park, N.-G.; Tilley, S. D.; Fan, H. J.; Grätzel, M. *Science* **2014,** *345*, 1593-1596.
[54] Sun, K.; Liu, R.; Chen, Y.; Verlage, E.; Lewis, N. S.; Xiang, C. *Adv. Energy Mater.* **2016,** *6*, 1600379.
[55] Ding, X.; Zhang, L.; Wang, Y.; Liu, A.; Gao, Y. *Coord. Chem. Rev.* **2018,** *357*, 130-143.
[56] Zong, R.; Thummel, R. P. *J. Am. Chem. Soc.* **2005,** *127*, 12802-12803.
[57] Hetterscheid, D. G. H.; Reek, J. N. H. *Angew. Chem. Int. Ed.***2012,** *51*, 9740-9747.
[58] Cao, R.; Lai, W.; Du, P. *Energy Environ. Sci.* **2012,** *5*, 8134-8157.
[59] Watabe, S.; Tanahashi, Y.; Hirahara, M.; Yamazaki, H.; Takahashi, K.; Mohamed, E. A.; Tsubonouchi, Y.; Zahran, Z. N.; Saito, K.; Yui, T.; Yagi, M. *Inorg. Chem.* **2019,** *58*, 12716-12723.
[60] Kishore, R. S. K.; Kel, O.; Banerji, N.; Emery, D.; Bollot, G.; Mareda, J.; Gomez-Casado, A.; Jonkheijm, P.; Huskens, J.; Maroni, P.; Borkovec, M.; Vauthey, E.; Sakai, N.; Matile, S. *J. Am. Chem. Soc.* **2009,** *131*, 11106-11116.

[61] Swierk, J. R.; Méndez-Hernández, D. D.; McCool, N. S.; Liddell, P.; Terazono, Y.; Pahk, I.; Tomlin, J. J.; Oster, N. V.; Moore, T. A.; Moore, A. L.; Gust, D.; Mallouk, T. E. *Proc. Natl. Acad. Sci.* **2015,** *112*, 1681-1686.

[62] Belić, J.; van Beek, B.; Menzel, J. P.; Buda, F.; Visscher, L. *J. Phys. Chem. A* **2020,** *124*, 6380-6388.

[63] Ambrosio, F.; Martsinovich, N.; Troisi, A. *J. Phys. Chem. Lett.* **2012,** *3*, 1531-1535.

[64] Zhang, L.; Cole, J. M. *ACS Appl. Mater. Interfaces* **2015,** *7*, 3427-3455.

[65] Materna, K. L.; Crabtree, R. H.; Brudvig, G. W. *Chem. Soc. Rev.* **2017,** *46*, 6099-6110.

[66] Monti, A.; Negre, C. F. A.; Batista, V. S.; Rego, L. G. C.; de Groot, H. J. M.; Buda, F. *J. Phys. Chem. Lett.* **2015,** *6*, 2393-2398.

[67] Monti, A.; de Groot, H. J. M.; Buda, F. *J. Phys. Chem. C* **2014,** *118*, 15600-15609.

[68] Emetere, M. E. Introduction to Computational Techniques. In *Environmental Modeling Using Satellite Imaging and Dataset Re-processing*, Springer International Publishing: Cham, 2019; pp. 19-37.

[69] Xu, P.; McCool, N. S.; Mallouk, T. E. *Nano Today* **2017,** *14*, 42-58.

[70] Wang, D.; Eberhart, M. S.; Sheridan, M. V.; Hu, K.; Sherman, B. D.; Nayak, A.; Wang, Y.; Marquard, S. L.; Dares, C. J.; Meyer, T. J. *Proc. Natl. Acad. Sci.* **2018,** *115*, 8523-8528.

[71] Chabi, S.; Papadantonakis, K. M.; Lewis, N. S.; Freund, M. S. *Energy Environ. Sci.* **2017,** *10*, 1320-1338.

[72] Ran, J.; Wu, L.; He, Y.; Yang, Z.; Wang, Y.; Jiang, C.; Ge, L.; Bakangura, E.; Xu, T. *J. Membr. Sci.* **2017,** *522*, 267-291.

[73] Janna Olmos, J. D.; Becquet, P.; Gront, D.; Sar, J.; Dąbrowski, A.; Gawlik, G.; Teodorczyk, M.; Pawlak, D.; Kargul, J. *RSC Adv.* **2017,** *7*, 47854-47866.

[74] Born, M.; Oppenheimer, R. *Ann. Phys.* **1927,** *389*, 457-484.

[75] Kohn, W. *Rev. Mod. Phys.* **1999,** *71*, 1253-1266.

[76] Hohenberg, P.; Kohn, W. *Phys. Rev.* **1964,** *136*, B864-B871.

[77] Kohn, W.; Sham, L. J. *Phys. Rev.* **1965,** *140*, A1133-A1138.

[78] Cohen, A. J.; Mori-Sánchez, P.; Yang, W. *Chem. Rev.* **2012,** *112*, 289-320.

[79] Swart, M.; Ehlers, A. W.; Lammertsma, K. *Mol. Phys.* **2004,** *102*, 2467-2474.

[80] te Velde, G.; Bickelhaupt, F. M.; Baerends, E. J.; Fonseca Guerra, C.; van Gisbergen, S. J. A.; Snijders, J. G.; Ziegler, T. *J. Comput. Chem.* **2001,** *22*, 931-967.

[81] ADF2017, SCM. Theoretical Chemistry, Vrije Universiteit, Amsterdam, The Netherlands, http://www.scm.com.

[82] CPMD, http://www.cpmd.org, Copyright IBM Corp., 1990–2019; Copyright MPI für Festkörperforschung Stuttgart, 1997–2001.

[83] Kleinman, L.; Bylander, D. M. *Phys. Rev. Lett.* **1982,** *48*, 1425-1428.

[84] Lin, I. C.; Coutinho-Neto, M. D.; Felsenheimer, C.; von Lilienfeld, O. A.; Tavernelli, I.; Rothlisberger, U. *Phys. Rev. B* **2007,** *75*, 205131.

[85] Grimme, S.; Ehrlich, S.; Goerigk, L. *J. Comput. Chem.* **2011,** *32*, 1456-1465.

[86] Car, R.; Parrinello, M. *Phys. Rev. Lett.* **1985,** *55*, 2471-2474.

[87] Marx, D.; Hutter, J., *Ab initio molecular dynamics: basic theory and advanced methods*. Cambridge University Press, **2009**.

[88] Ciccotti, G.; Ferrario, M. *Mol. Simul.* **2004,** *30*, 787-793.

[89] Ensing, B.; Meijer, E. J.; Blöchl, P. E.; Baerends, E. J. *J. Phys. Chem. A* **2001,** *105*, 3300-3310.

[90] Sprik, M.; Ciccotti, G. *J. Chem. Phys.* **1998,** *109*, 7737-7744.

[91] Eyring, H. *J. Chem. Phys.* **1935,** *3*, 107-115.

[92] Laidler, K. J.; King, M. C. *J. Phys. Chem.* **1983,** *87*, 2657-2664.

[93] Hammes-Schiffer, S.; Tully, J. C. *J. Chem. Phys.* **1995,** *103*, 8528-8537.

Chapter

1